HHS Public Access

Author manuscript

Immunity. Author manuscript; available in PMC 2016 November 17.

Published in final edited form as:

Immunity. 2015 November 17; 43(5): 933–944. doi:10.1016/j.immuni.2015.11.001.

Isoforms of the RNA editing enzyme ADAR1 independently control nucleic acid sensor MDA5-driven autoimmunity and multi-organ development

Kathleen Pestal[1], **Cory C. Funk**[2], **Jessica M. Snyder**[3], **Nathan D. Price**[2], **Piper M. Treuting**[3], and **Daniel B. Stetson**[1,*]

[1]Department of Immunology, University of Washington School of Medicine, Seattle, WA 98195 USA

[2]Institute for Systems Biology, Seattle, WA 98195 USA

[3]Department of Comparative Medicine, University of Washington School of Medicine, Seattle, WA 98195 USA

Summary

Mutations in the *ADAR* gene that encodes the ADAR1 RNA editing enzyme cause Aicardi-Goutières Syndrome (AGS), a severe autoimmune disease associated with an aberrant type I interferon response. How ADAR1 prevents autoimmunity remains incompletely defined. Here, we demonstrate that ADAR1 is a specific and essential negative regulator of the MDA5-MAVS RNA sensing pathway. Moreover, we uncovered a MDA5-MAVS-independent function for ADAR1 in the development of multiple organs. We showed that the p150 isoform of ADAR1 uniquely regulated the MDA5 pathway, whereas both the p150 and p110 isoforms contributed to development. Abrupt deletion of ADAR1 in adult mice revealed that both of these functions were required throughout life. Our findings delineate genetically separable roles for both ADAR1 isoforms *in vivo*, with implications for the human diseases caused by *ADAR* mutations.

Graphical Abstract

*Correspondence: stetson@uw.edu; phone: 206-543-6633; fax: 206-221-5433.

Author Contributions

K.P. and D.B.S. conceived of the project and wrote the manuscript. K.P. performed the experiments. C.C.F. and N.D.P. analyzed RNA-Seq data. J.M.S. and P.M.T. performed the histological analyses. All authors edited the manuscript.

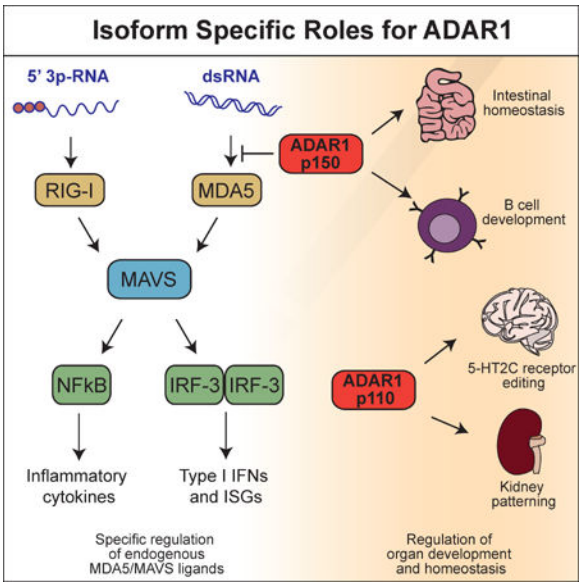

Introduction

Intracellular detection of foreign nucleic acids initiates the production of type I interferons (IFNs) and is essential for host defense against virus infection (Goubau et al., 2013). Characterization of the RIG-I-like receptor-MAVS RNA sensing pathway and the cGAS-STING DNA sensing pathway has illuminated the earliest events of virus detection in molecular detail (Wu and Chen, 2014). Given the millions of molecules of RNA and the billions of base pairs of genomic DNA present in all nucleated cells, negative regulation of these pathways has emerged as a key mechanism to prevent autoreactivity. Much of our understanding of this regulation comes from the genetic dissection of a severe human autoimmune disease called Aicardi-Goutières Syndrome (AGS), first described over 30 years ago as a monogenic disorder associated with the aberrant production of type I IFNs (Aicardi and Goutieres, 1984; Lebon et al., 1988). Crow and colleagues have identified seven human genes that are mutated in AGS, providing a framework for studying the mechanisms that limit activation of intracellular nucleic acid sensors: *TREX1, RNASEH2A, RNASEH2B, RNASEH2C, SAMHD1, ADAR, and IFIH1 (MDA5)* (Crow et al., 2015; Crow and Manel, 2015).

Among the best characterized of the AGS enzymes is Trex1, a cytosolic DNA exonuclease. Trex1-deficient mice develop lethal autoimmune disease that is entirely dependent on cGAS, STING, the IRF3 transcription factor, the type I IFN receptor, and lymphocytes, thus defining Trex1 as a specific and essential negative regulator of the intracellular DNA sensing pathway (Ablasser et al., 2014; Gall et al., 2012; Gao et al., 2015; Gray et al., 2015; Stetson et al., 2008). Similarly, SAMHD1 is a dNTP phosphohydrolase that prevents cDNA synthesis by retroviral reverse transcriptase enzymes, strongly suggesting that the cGAS-STING pathway also drives autoimmunity in AGS caused by *SAMHD1* mutations (Goldstone et al., 2011; Hrecka et al., 2011; Laguette et al., 2011; Rehwinkel et al., 2013). Interestingly, identification of the innate immune pathway regulated by RNase H2 is

complicated by the early embryonic lethality of RNase H2-deficient mice, caused by accumulation of ribonucleotides in genomic DNA and massive genome instability (Hiller et al., 2012; Reijns et al., 2012).

The identification of AGS mutations in the *ADAR* gene that encodes the ADAR1 enzyme revealed a disease mechanism that does not fit into the cGAS-STING pathway (Rice et al., 2012). The *ADAR* gene in mammals encodes two open reading frames that give rise to two protein isoforms: a p110 isoform that is constitutively and ubiquitously expressed; and a larger p150 isoform that is IFN-inducible and contains two complete zDNA-binding domains that are not found in p110 (Bass, 2002; Schwartz et al., 1999). ADAR1 is a deaminase that converts adenosine to inosine (A to I) within double-stranded regions of RNA (Bass, 2002). In coding regions, inosine is decoded as guanosine (G), leading to amino acid changes or stop codon read-through at edited sites. In introns of mRNAs, editing can create or destroy splice acceptor sites. In double-stranded regions of RNA, the I-U base pair is unstable compared to the parental A-U base pair, leading to changes in secondary structure of RNA that can result in degradation (Wang et al., 2013). In mammals, ADAR1 edits coding RNAs (Hartner et al., 2004), microRNAs (Yang et al., 2006), and the RNA transcripts of the prolific SINE retroelements (Osenberg et al., 2010). Interestingly, ADAR1 deficiency in mice results in embryonic lethality, accompanied by massive overproduction of type I IFNs and hematopoietic failure (Hartner et al., 2004; Hartner et al., 2009; Wang et al., 2000). A number of mechanisms have been proposed to explain the dramatic phenotype of $Adar^{-/-}$ mice, including roles for ADAR1 in modulation of microRNA biogenesis (Ota et al., 2013), control of the length of mRNA 3′ untranslated regions (UTRs; Bahn et al., 2015), physical sequestration of RNAs from RIG-I (Yang et al., 2014), and the direct suppression of RIG-I and MDA5 activity by RNAs that contain inosine (Vitali and Scadden, 2010). In addition, a recent study identified live births of $Adar^{-/-}Mavs^{-/-}$ mice (Mannion et al., 2014). However, the precise innate immune pathways regulated by ADAR1 and the contributions of these pathways to the phenotypes of $Adar^{-/-}$ mice remain undefined.

In this study, we define ADAR1 as a specific negative regulator of the MDA5-MAVS pathway. Moreover, we reveal an essential role for ADAR1 in multi-organ development and homeostasis that is independent of the MDA5-MAVS pathway. We show that the two isoforms of ADAR1 contribute independently to each of these functions.

Results

ADAR1 is a specific negative regulator of the MDA5-MAVS pathway

To define the innate immune receptor(s) and signaling pathways responsible for the embryonic lethality of $Adar^{-/-}$ mice, we analyzed over 700 live births of $Adar^{+/-}$ intercrosses, alone and on four additional genetic backgrounds: *Tmem173* $(Sting)^{-/-}$, $Mavs^{-/-}$, *Ifih1* $(Mda5)^{-/-}$, *and Ddx58* $(Rigi)^{+/-}$. Consistent with previous reports defining fully penetrant embryonic lethality of $Adar^{-/-}$ mice (Hartner et al., 2004; Wang et al., 2000), we found no live births of $Adar^{-/-}$ mice (Figure 1A). Similarly, no $Adar^{-/-}Tmem173^{-/-}$ mice were born, and the frequencies of live $Adar^{+/+}Tmem173^{-/-}$ and $Adar^{+/-}Tmem173^{-/-}$ mice were indistinguishable from mice born from the $Adar^{+/-}$ intercross, formally demonstrating that the STING pathway plays no role in the phenotypes

associated with ADAR1 deficiency (Figure 1B). In contrast, and consistent with a recent report (Mannion et al., 2014), *Adar*$^{-/-}$*Mavs*$^{-/-}$ mice were born at frequencies that were statistically indistinguishable from expected Mendelian ratios (Figure 1C). Thus, the MAVS pathway, and not the STING pathway, drives the embryonic lethality of *Adar*$^{-/-}$ mice.

We next evaluated intercrosses of *Adar*$^{+/-}$ mice with mice lacking the two principal RNA sensors upstream of MAVS: MDA5 (*Ifih1*) and RIG-I (*Ddx58*; Kato et al., 2006). Remarkably, *Adar*$^{-/-}$*Ifih1*$^{-/-}$ mice were born at expected Mendelian frequencies (Figure 1D). The *Adar-Ddx58* cross was complicated by the embryonic lethality of most *Ddx58*$^{-/-}$ mice (Kato et al., 2005), which occurs for reasons that remain poorly defined. Therefore, we bred *Adar*$^{+/-}$ mice to *Ddx58*$^{+/-}$ mice and analyzed over 300 live births. We recovered only two *Ddx58*$^{-/-}$ single mutant mice and no *Adar*$^{-/-}$*Ddx58*$^{-/-}$ mice (Figure 1E).

We performed timed matings of *Adar*$^{+/-}$ mice on the four backgrounds described above, harvested embryos at day 11.5 of development (E11.5, before the onset of lethality in *Adar*$^{-/-}$ mice), and assessed the innate immune response using quantitative RT-PCR analysis of six interferon stimulated genes (ISGs). We found that MAVS deficiency completely reversed the elevated ISG signature of *Adar*$^{-/-}$ embryos, but STING deficiency had no effect (Figure 2A). Moreover, and identical to *Adar*$^{-/-}$*Mavs*$^{-/-}$ embryos, we found that *Adar*$^{-/-}$*Ifih1*$^{-/-}$ embryos also lacked the increased ISG expression seen in *Adar*$^{-/-}$ embryos. Importantly, the single *Adar*$^{-/-}$*Ddx58*$^{-/-}$ embryo that we recovered had elevated ISG expression that was identical to control *Adar*$^{-/-}$*Ddx58*$^{+/+}$ embryos (Figure 2B). Taken together, these data define MDA5-MAVS, and not RIG-I-MAVS, as the specific innate immune pathway responsible for both the dysregulated ISG expression and the embryonic lethality of *Adar*$^{-/-}$ mice.

To extend our findings to human cells, we used a lenti-CRISPR approach to disrupt the endogenous *ADAR* gene in HEK 293T cells. We designed a guide RNA to target an exon shared by both isoforms of ADAR1, transduced and selected targeted cells, and then derived a clonal line of *ADAR*-null cells with frameshift mutations in all three alleles of *ADAR* (Figure 3A; HEK 293T cells are triploid for chromosome 3). We confirmed by western blot that these *ADAR*-null cells lacked expression of both isoforms of ADAR1 protein (Figure 3B). We then introduced expression vectors for either RIG-I or MDA5 into these cells or control cells, and measured the IFN response using an interferon-stimulated response element (ISRE)-luciferase reporter. We found that RIG-I responded identically in control and *ADAR*-null cells at each concentration of transfected expression vector (Figure 3C). Remarkably, the MDA5-activated IFN response was enhanced in *ADAR*-null HEK 293T cells compared to control cells at all concentrations of plasmid (Figure 3C). These findings, together with our analysis of *Adar*$^{-/-}$ mice and embryos, strongly suggest that ADAR1 deficiency results in the accumulation of endogenous, immunostimulatory RNAs that are specifically detected by MDA5 and not by RIG-I.

MAVS-dependent and MAVS-independent gene expression changes in *Adar−/−* embryos

To assess global changes in gene expression caused by ADAR1 deficiency beyond the specific ISGs analyzed in Figure 2, we performed RNA-Seq analysis of gene expression in whole E11.5 embryos, comparing *Adar*$^{-/-}$ to *Adar*$^{+/+}$ embryos, as well as *Adar*$^{-/-}$*Mavs*$^{-/-}$

to *Adar*$^{+/+}$*Mavs*$^{-/-}$ embryos (Figure 4 and Supplementary Tables 1 and 2). In both cases, the great majority of dysregulated genes exhibited increased expression in the *Adar*$^{-/-}$ embryos compared to respective controls, suggesting that ADAR1 is primarily a negative regulator of gene expression (Figure 4A, 4B). We found over 900 genes with significantly different expression levels in *Adar*$^{-/-}$ versus *Adar*$^{+/+}$ embryos, 180 of which were ISGs (Figure 4A). As expected, the increased expression of nearly all of these ISGs was restored to normal levels in the *Adar*$^{-/-}$*Mavs*$^{-/-}$ embryos (Figure 4A, 4B, red dots). However, and unexpectedly, we identified over 200 genes with similarly dysregulated expression in both *Adar*$^{-/-}$ and *Adar*$^{-/-}$*Mavs*$^{-/-}$ embryos compared to their respective controls (Figure 4A–4C, blue dots). Bioinformatics analysis of these genes revealed highly enriched biological processes and transcription factor networks controlled by ADAR1 in a MAVS-independent fashion. These included genes involved in lipid metabolism and transport, associated with up-regulation of PPAR-γ transcriptional targets in *Adar*$^{-/-}$ embryos (Figure 4D, 4E). Moreover, we identified targets of the TCF1, TCF14, TCF3, and HOXA13 transcription factors that control cell fate specification during development (Figure 4D, 4E). Importantly, we found no evidence for residual inflammatory gene expression in *Adar*$^{-/-}$*Mavs*$^{-/-}$ embryos (Fig. 4D, 4E), suggesting that the entire dysregulated innate immune response caused by ADAR1 deficiency depends on MAVS signaling. Thus, ADAR1 controls expression of two classes of genes: the first class is innate immune response genes driven by MAVS signaling, whereas the second class is MAVS-independent and implicated in development and metabolism.

MDA5-MAVS-independent control of multi-organ development by ADAR1

Consistent with the identification of a substantial set of MAVS-independent genes regulated by ADAR1 (Figure 4), we observed a fully penetrant postnatal mortality in both *Adar*$^{-/-}$*Mavs*$^{-/-}$ mice and *Adar*$^{-/-}$*Ifih1*$^{-/-}$ mice, with the majority of neonates dying by two days of age (Figure 5A, 5B). We analyzed the phenotypes of the small number of *Adar*$^{-/-}$*Mavs*$^{-/-}$ mice that survived past one week of age, comparing them to *Adar*$^{+/+}$*Mavs*$^{-/-}$ littermates. The double knockout mice were severely runted compared to their *Mavs*$^{-/-}$ littermates, but they appeared to be feeding, as evidenced by the presence of milk in their stomachs (data not shown). However, the *Adar*$^{-/-}$*Mavs*$^{-/-}$ mice were largely unresponsive and immobile, with a “trembling” phenotype (Supplementary Video 1). We performed a thorough histological analysis of tissues and organs in three mice of each genotype, revealing a number of novel, MAVS-independent developmental phenotypes caused by ADAR1 deficiency. First, the kidneys of *Adar*$^{-/-}$*Mavs*$^{-/-}$ mice had a profound change in architecture, with multiple discrete lobes of the outer medulla and marked disorganization of the tubules in the corticomedullary junction (Figure 5C). This contrasts with the single-lobed outer medulla of normal rodent kidneys, revealing an unexpected role for ADAR1 in regulation of kidney patterning during development. Second, we observed a dramatic dysregulation of gastrointestinal homeostasis in *Adar*$^{-/-}$*Mavs*$^{-/-}$ mice (Figure 5C). This phenotype was apparent throughout the intestine, although most pronounced in the small intestine. Intestinal lesions included moderate superficial enterocyte vacuolation, mild to moderate villar fusion, and extensive apoptosis of enterocytes that was especially pronounced in the crypts, with mild proliferation and mild mixed inflammation (enteritis; Figure 5C). Third, we found a near complete lack of organized lymphoid follicles in both

lymph nodes and spleens of *Adar*$^{-/-}$*Mavs*$^{-/-}$ mice, on both histology (Figure 5C) and immunofluorescence microscopy performed to localize T cells and B cells (Figure 5D). In the spleens of *Adar*$^{-/-}$*Mavs*$^{-/-}$ mice, there was extramedullary hematopoiesis of both myeloid and erythroid lineages (Figure 5C). Fourth, flow cytometry analysis of splenocytes revealed a dramatic reduction in the frequency of mature B cells, but relatively normal numbers of T cells, as well as increased frequencies of CD11c+ dendritic cells (Figure 5E). These phenotypes of *Adar*$^{-/-}$*Mavs*$^{-/-}$ mice reveal an essential role for ADAR1 in the development and homeostasis of multiple organs, independent of its role as a negative regulator of the MDA5-MAVS-mediated antiviral response. Importantly, we demonstrate that the failure of hematopoiesis in *Adar*$^{-/-}$ mice is an indirect consequence of the aberrant, MDA5-MAVS-dependent antiviral response, revealing instead a selective, MDA5-MAVS-independent role for ADAR1 in development of B cells.

Independent contributions of ADAR1 isoforms to regulation of MDA5-MAVS and development

We evaluated the relative *in vivo* contributions of the p150 and p110 isoforms of ADAR1 to regulation of MDA5-MAVS-dependent autoimmunity versus MDA5-MAVS-independent organ development. To do this, we studied *Adar p150*$^{-/-}$ mice, which were generated by targeted disruption of the unique promoter and first exon that encodes the amino terminus of the p150 isoform (Ward et al., 2011). *Adar p150*$^{-/-}$ mice are embryonic lethal, similar to *Adar*$^{-/-}$ mice that lack both the p150 and p110 isoforms of ADAR1 (Ward et al., 2011). Given that the embryonic lethality of *Adar*$^{-/-}$ mice is entirely MDA5- and MAVS-dependent (Figure 1), we hypothesized that the ADAR1 p150 isoform might specifically regulate the MDA5-MAVS pathway. We performed western blot analysis of *Adar p150*$^{+/-}$ and *Adar p150*$^{-/-}$ MEF extracts and confirmed the absence of p150 protein in these cells, but normal levels of the p110 isoform (Figure 6A). Next, we intercrossed *Adar p150*$^{+/-}$*Mavs*$^{-/-}$ mice and observed complete rescue of the *Adar p150*$^{-/-}$*Mavs*$^{-/-}$ mice to birth, demonstrating that the p150 isoform of ADAR1 is the unique and essential negative regulator of the MAVS pathway (Figure 6B). Remarkably, and unlike the *Adar*$^{-/-}$*Mavs*$^{-/-}$ mice that died shortly after birth (Figure 5A), most of the *Adar p150*$^{-/-}$*Mavs*$^{-/-}$ mice survived to weaning (Figure 6C). Moreover, these mice were active and mobile, ate solid food, and did not tremble, although they were smaller than their control littermates (Supplementary video 1). We performed a histological analysis of *Adar p150*$^{-/-}$*Mavs*$^{-/-}$ mice, comparing them to *Adar*$^{-/-}$*Mavs*$^{-/-}$ mice (Figure 5) and to controls. We found that the kidney abnormalities that were present in the *Adar*$^{-/-}$*Mavs*$^{-/-}$ mice were largely absent in *Adar p150*$^{-/-}$*Mavs*$^{-/-}$ mice, demonstrating that p110 is a specific regulator of kidney development (Figure 6D). However, the dysregulated intestinal homeostasis was similar between *Adar p150*$^{-/-}$*Mavs*$^{-/-}$ mice compared to the *Adar*$^{-/-}$*Mavs*$^{-/-}$ mice (Figure 6D). Moreover, the lymph nodes and spleens of *Adar p150*$^{-/-}$*Mavs*$^{-/-}$ mice were still devoid of lymphoid follicles (Figure 6D). Consistent with this, we observed reduced numbers of peripheral B cells and increased numbers of CD11c+ myeloid cells in *Adar p150*$^{-/-}$*Mavs*$^{-/-}$ mice (Figure 6E), identical to *Adar*$^{-/-}$*Mavs*$^{-/-}$ mice (Figure 5E). Thus, expression of the p110 isoform of ADAR1 in *Adar p150*$^{-/-}$*Mavs*$^{-/-}$ mice is sufficient to restore kidney development, but not intestinal homeostasis or B cell development.

We next examined editing of the mRNA encoding the 5-HT2C serotonin receptor that mediates numerous actions of serotonin in the central nervous system, including feeding and sleep behavior, as well as inhibition of neuronal excitability (Frank et al., 2002; Tecott et al., 1995). A prior study identified ADAR1-dependent editing at two specific adenosines within the 5-HT2C open reading frame in cultured embryonic neurons, termed the "A" and "B" sites (Hartner et al., 2004). We therefore measured editing of these sites in cDNAs prepared from brains of ~20 day old *Adar*$^{-/-}$*Mavs*$^{-/-}$ and *Adar p150*$^{-/-}$*Mavs*$^{-/-}$ mice. Consistent with the prior study, we found that both the "A" and "B" sites of 5-HT2C mRNAs were extensively edited in control *Mavs*$^{-/-}$ mice, and that this editing was absent in *Adar*$^{-/-}$*Mavs*$^{-/-}$ mice (Figure 6F). Interestingly, the *Adar p150*$^{-/-}$*Mavs*$^{-/-}$ mice had normal levels of editing at these sites, demonstrating that ADAR1 p110 is both necessary and sufficient for editing of these sites *in vivo* (Figure 6F). This finding reveals a specific editing event mediated by p110 and not by p150. These, as well as other potential p110-specific editing events that remain to be identified, may contribute to the phenotypic differences between *Adar*$^{-/-}$*Mavs*$^{-/-}$ mice and *Adar p150*$^{-/-}$*Mavs*$^{-/-}$ mice. Together, these data demonstrate independent roles for ADAR1 isoforms: the p150 isoform regulates the MDA5-MAVS pathway, and both isoforms contribute to development.

ADAR1 controls both innate immunity and homeostasis in adult mice

Our findings demonstrating roles for ADAR1 in controlling both the MDA5-MAVS pathway and multi-organ development led us to test whether these functions are similarly required in adult mice. We crossed mice with a floxed *Adar* allele (*Adar*$^{fl/fl}$; (Hartner et al., 2009) to mice expressing a tamoxifen-inducible Ert2-Cre transgene under the control of the broadly expressed *UBC* promoter (Ruzankina et al., 2007), on both *Mavs*$^{+/+}$ and *Mavs*$^{-/-}$ backgrounds. We treated these mice daily for three days by intraperitoneal injection of tamoxifen, which resulted in widespread deletion of the floxed *Adar* alleles in Ert2-Cre-expressing mice as measured by genotyping of ear tissue (Figure 7A). We found that the tamoxifen injections resulted in a drop in body temperature in all treated mice, regardless of Cre expression or *Adar* genotype (Figure 7B). One day after the third tamoxifen treatment, and only four days after the initial treatment, we found that the *Adar*$^{fl/fl}$*Mavs*$^{+/+}$Ert2-Cre-expressing mice had an exacerbated reduction in body temperature (Figure 7B), were hunched and unresponsive, and required immediate euthanasia. We measured the abundance of 32 serum cytokines and chemokines in these mice and controls and found dramatically elevated levels of many of them, including TNFα, CXCL10, and IL-10, thus revealing a profound systemic inflammatory response instigated by abrupt *Adar* deletion on a *Mavs*$^{+/+}$ background (Figure 7C). In contrast, the *Adar*$^{fl/fl}$*Mavs*$^{-/-}$Ert2-Cre-expressing mice recovered body temperature after cessation of tamoxifen treatments and appeared healthy for five more days (Figure 7B). At day 8 post treatment, we noted that these mice were abnormal compared to controls, so we prepared these mice for serum cytokine analysis and histological evaluation. We found that the systemic cytokine response was absent in the *Adar*$^{fl/fl}$*Mavs*$^{-/-}$Ert2-Cre-expressing mice, demonstrating that MAVS controls the entire inflammatory response caused by *Adar* deletion in adult mice (Figure 7C). However, we found that the small intestines of mice with *Adar* deletion on a *Mavs*$^{-/-}$ background were shortened relative to Cre-expressing control mice, and their colons were thickened and devoid of formed stools (Figure 7D). Histological analysis revealed a disruption of intestinal

homeostasis in these mice (Figure 7E, 7F), reminiscent of the intestinal phenotype of *Adar*$^{-/-}$*Mavs*$^{-/-}$ and *Adar p150*$^{-/-}$*Mavs*$^{-/-}$ mice. Together, these data demonstrate that the requirement for ADAR1 in regulation of both the MDA5-MAVS pathway and tissue homeostasis is maintained in adult mice.

Discussion

Our findings reveal two important roles for ADAR1. First, ADAR1 is a specific and essential negative regulator of the MDA5- and MAVS-dependent antiviral response. Second, ADAR1 is a key regulator of multi-organ development and homeostasis, independent of the MDA5-MAVS pathway. These roles are both genetically and temporally separable, with the MDA5-MAVS pathway entirely responsible for the embryonic lethality, and the MDA5-MAVS-independent pathway responsible for the postnatal mortality of *Adar*$^{-/-}$ mice. Moreover, we demonstrate that ADAR1 isoforms independently contribute to these two functions, with the p150 isoform essential for regulation of the MDA5-MAVS pathway, and the p110 isoform contributing to development. Finally, we demonstrate that ADAR1 regulates both innate immunity and tissue homeostasis in adult mice.

Our data provide insight into the *ADAR* gene mutations in humans that cause AGS (Crow et al., 2015; Rice et al., 2012). The regulation of the MDA5-MAVS pathway by ADAR1 p150, and not the RIG-I-MAVS pathway, strongly suggests that ADAR1 p150 modifies a discrete pool of RNAs to prevent their specific detection by MDA5. Moreover, our findings reveal a clear genetic pathway linking the *ADAR* and *IFIH1* mutations found in AGS (Rice et al., 2014; Rice et al., 2012), a rationale for the *ADAR* AGS mutations that affect only the p150 isoform of ADAR1 (Crow et al., 2015; Rice et al., 2012), and a biological framework for understanding the numerous *IFIH1* gene polymorphisms in humans that are associated with type I diabetes, systemic lupus erythematosus, and Graves disease (Gateva et al., 2009; Nejentsev et al., 2009; Smyth et al., 2006; Sutherland et al., 2007). Given the embryonic lethality and robust IFN signature of *Adar*$^{-/-}$ mice, as well as the rapid MAVS-dependent inflammatory response that arises after abrupt *Adar* deletion in adults, we propose that the ADAR1-regulated endogenous MDA5 RNA ligands are broadly expressed, highly immunostimulatory, or both. Definitive identification of these RNAs will provide insight into the elusive ligand specificity of MDA5 (Wu et al., 2013), with implications for the underlying mechanisms of self/non-self discrimination by intracellular nucleic acid sensors.

Analysis of *Adar*$^{-/-}$ and *Adar p150*$^{-/-}$ mice on a *Mavs*$^{-/-}$ background revealed isoform-specific contributions of ADAR1 to kidney development, intestinal homeostasis, B cell development, and 5-HT2C serotonin receptor editing. Further work will be required to determine whether these functions are mediated by “precision editing” of adenosines in mRNA open reading frames that result in new coding potential (as is the case for 5-HT2C), or whether some of these functions require previously described roles for ADAR1 in control of micro-RNA processing, mRNA stability, or mRNA 3′-UTR length (Ota et al., 2013; Bahn et al., 2015).

Importantly, no AGS patients are homozygous for null alleles of *ADAR*, and most AGS-mutant ADAR1 enzymes are competent for RNA editing *in vitro* (Rice et al., 2012). Distinct

ADAR mutations in humans also cause dyschromatosis symmetrica hereditaria (DSH; OMIM 127400; (Hayashi and Suzuki, 2013) and bilateral striatal necrosis (BSN; OMIM 271930; (Livingston et al., 2014). Some DSH and BSN cases are associated with a mild IFN signature that is less pronounced compared to AGS with *ADAR* mutations, but the clinical presentations of DSH and BSN differ significantly from classical AGS (Livingston et al., 2014; Rice et al., 2012). Our identification of an MDA5-MAVS-independent role for ADAR1 in development and tissue homeostasis may shed light on the various human phenotypes associated with *ADAR* mutations. We propose that the more than 150 known mutations in *ADAR* represent a spectrum of effects on ADAR1 regulation of the MDA5-MAVS pathway versus ADAR1 control of tissue homeostasis. Specific disease presentations may reflect the extent to which each pathway is compromised by a particular mutation. For example, AGS mutations likely impact primarily the MDA5-MAVS response controlled by the p150 isoform, leaving the developmental roles of ADAR intact.

A very recent study by Walkley and colleagues described the phenotype of knockin mice with a point mutation in the *Adar* gene that disrupts catalytic activity (E861A; (Liddicoat et al., 2015). Consistent with our findings, they identified two individual $Adar^{E861A/E861A}Ifih1^{-/-}$ mice that were rescued to birth. Interestingly, and in contrast to our data demonstrating fully penetrant postnatal mortality in $Adar^{-/-}Ifih1^{-/-}$ mice, the rescued $Adar^{E861A/E861A}Ifih1^{-/-}$ mice were largely normal in appearance, with no evident gross lesions. It is tempting to speculate that the differences in postnatal phenotypes revealed in our study and theirs may reflect an important distinction between the catalytic mutant and the null allele of *Adar*. A direct comparison of the null allele and the catalytic mutant allele of *Adar* on an $Ifih1^{-/-}$ or $Mavs^{-/-}$ background would resolve this issue.

In summary, we have identified independent roles for ADAR1 isoforms in regulation of the antiviral response and control of tissue development and homeostasis, with implications for the human diseases caused by *ADAR* mutations.

Experimental Procedures

Mice

$Adar^{fl/fl}$ mice were kindly provided by Dr. Stuart Orkin (Hartner et al., 2009) and were bred to B6.129S4-$Meox2^{tm1(cre)Sor}$ mice to delete the *Adar* allele in the germline, and to B6;129S-Tg(UBC-cre/ERT2)1Ejb to allow for tamoxifen-induced widespread deletion of *Adar* in adult mice. Both Cre-expressing mouse lines were purchased from the Jackson Laboratory (stock numbers 003755 and 008085). The $Adar^{+/-}$ mice resulting from the B6.129S4-$Meox2^{tm1(cre)Sor}$ cross were subsequently bred to $Tmem173^{-/-}$ ($Sting^{-/-}$) mice (Ishikawa et al., 2009), $Mavs^{-/-}$ mice (Gall et al., 2012), $Ddx58^{-/-}$ ($Rigi^{-/-}$) mice (Kato et al., 2005), or $Ifih1^{-/-}$ ($Mda5^{-/-}$) mice (Gitlin et al., 2006). *Adar* $p150^{+/-}$ gametes were generously provided by Dr. M. B. A. Oldstone (Ward et al., 2011). Sentinel mice (Crl:CD1[ICR]; Charles River, Wilmington, MA) were tested quarterly for endo- and ectoparasites, mouse hepatitis virus, mouse parvovirus, and rotavirus; and tested annually for *Mycoplasma pulmonis*, pneumonia virus of mice, reovirus 3, Sendai virus, and Theiler murine encephalomyelitis virus. All experiments were done in accordance with the Institutional Animal Care and Use Committee guidelines of the University of Washington.

Histology

Tissues were fixed in 10% neutral buffered formalin, paraffin embedded, cut into 4-5μm sections and routinely stained with hematoxylin and eosin. All tissues were coded to remove genotype identification. Tissues evaluated included lung, heart, esophagus, kidney, ureter, bladder, liver, pancreas, spleen, lymph nodes, salivary glands, stomach, small intestine, large intestine, and reproductive tract. Additionally, for the $Adar^{-/-}Mavs^{-/-}$ mice, decalcified cross sectional images of the skull and brain were also evaluated.

Flow cytometry and Cytokine Measurements

Single cell suspensions from spleen, bone marrow, thymus or blood were isolated and stained with antibodies for CD3 (145-2C11), CD4 (RM4-5), CD8β (H35-17.2), B220 (RA3-6B2), CD11c (N418), CD11b (M1/70), CD45.2 (104), and/or Ter119; Cells were analyzed with a FACSCanto (BD Biosciences) and analyzed with FlowJo software (TreeStar). Measurement of serum cytokines was performed using the Milliplex-70K-PX32 mouse cytokine/chemokine magnetic bead panel (Millipore), according to the manufacturers instructions.

Immunofluorescence microscopy

Spleens were frozen in Optimal Cutting Temperature (OCT) media (Sakura). Tissues were cut into 7-μm sections and treated with ice-cold acetone. Sections were stained with directly conjugated antibodies: CD8α (53–6.7, eBioscience), CD4 (RM4-5, eBioscience), and B220 (RA3-6B2, eBioscience). Nuclei were stained with 1 ug/mL DAPI. Stained slides were mounted with Prolong Gold antifade reagent (Life Technologies), imaged using a Nikon Eclipse 90i microscope and analyzed using Adobe Photoshop software.

Quantitative RT-PCR

Embryos were harvested into TRIzol (Life Technologies), homogenized through an 18-G needle attached to a 3 mL syringe, followed by RNA extraction according to manufacturer's instructions. RNA was treated with DNase (Ambion) and 1 μg was reverse-transcribed using RNA to cDNA EcoDry Premix (Double Primed) (Clontech). cDNA was used for PCR with EVA Green reagents (Bio-Rad Laboratories) on a Bio-Rad CFX96 Real-Time System. The abundance of each interferon-stimulated gene mRNA was normalized to that of HPRT mRNA and results were compared with genetic control embryos for calculation of relative induction.

The primers used were:

Cxcl10 Fwd:AAGTGCTGCCGTCATTTTCTGCCTC, *Cxcl10* Rev:CTTGATGGTCTTAGATTCCGGATTC;

Isg15 Fwd:GGTGTCCGTGACTAACTCCAT, *Isg15* Rev:TGGAAAGGGTAAGACCGTCCT;

Ifit1 Fwd:GCCATTCAACTGTCTCCTG, *Ifit1* Rev:GCTCTGTCTGTGTCATATACC;

Ifit2 Fwd:AGTACAACGAGTAAGGAGTCACT, *Ifit2* Rev:AGGCCAGTATGTTGCACATGG (Primer bank ID: 6680363a1);

Mx1 Fwd:GACCATAGGGGTCTTGACCAA, *Mx1* Rev:AGACTTGCTCTTTCTGAAAAGCC (Primer bank ID: 6996930a1);

Rsad2 Fwd:TGCTGGCTGAGAATAGCATTAGG, *Rsad2* Rev:GCTGAGTGCTGTTCCCATCT (Primer bank ID: 31543946a1);

Hprt Fwd:GTTGGATACAGGCCAGACTTTGTTG, *Hprt* Rev:GAGGGTAGGCTGGCCTATAGGCT (Spandidos et al., 2010);

Htr2c (5ht2c) Fwd:TGTCCCTAGCCATTGCTGATATG, *Htr2c* Rev:TGTCAACGGGATGAAGAATGCC.

Deletion of ADAR1 in adult mice

Tamoxifen-induced deletion was performed according to the protocol available from the Jackson Laboratory. In brief, tamoxifen (Sigma-Aldrich) was dissolved in corn oil (Sigma-Aldrich) at 20 mg/mL overnight at 37°C, filtered through a 0.22 μm Millex GP PES membrane and stored at 4°C. Mice were administered 100 μL of tamoxifen via i.p. injection once a day for three days. On day four, $Adar^{fl/fl}Mavs^{+/+}$ Cre-positive mice were moribund, so no further injections were given. Mice were sacrificed and analyzed by histology and flow cytometry.

RNA-Seq library preparation

Total RNA was harvest from embryos as described above. Ribosomal RNA was depleted using the RiboZero™ Magnetic Kit (Human/Mouse/Rat) from Illumina. Libraries were prepared from the Ribo-depleted RNA using the NEBNext® Ultra™ RNA Library Prep Kit for Illumina® (New England BioLabs) with the following modifications: Ribo-depleted RNA was fragmented for 5 min at 94°C to obtain >300bp fragments and first strand synthesis reaction was incubated for 50 min at 42°C. PCR Library enrichment was performed using the KAPA HiFi DNA Polymerase (KAPA Biosystems) with Illumina barcoded sequencing primers. Library size distribution was confirmed on an Agilent 2100 Bioanalyzer with a High Sensitivity DNA Chip (Agilent Technologies). Barcoded libraries were combined and sequenced with an Illumina NextSeq, resulting in approximately 60 million paired-end 150-base pair sequencing reads per embryo.

Alignment and analysis of RNA-Seq data

Fastq files were aligned using STAR 2.4.2a (Dobin et al., 2013), with the following parameters for the indices: STAR--runMode genomeGenerate--genomeDir /mnt/indices/--genomeFastaFiles /mnt/genome/Mus_musculus.GRCm38.dna.SORTED.fa--sjdbGTFfile /mnt/transcriptome/Mus_musculus.GRCm38.81.gtf--runThreadN 32 . Alignment was performed with the following parameters: STAR--genomeDir /mnt/indices/--readFilesIn /mnt2/data/run2/${i}_R1.fastq.gz /mnt2/data/run2/${i}_R2.fastq.gz--readFilesCommand zcat--runThreadN 32--outSAMtype BAM SortedByCoordinate--quantMode GeneCounts--outFilterMismatchNmax 30--outFileNamePrefix /mnt/results/run2/${i}.star.--outFilterMultimapNmax 20--outSAMattributes All.

All alignments were performed on Amazon EC2 c3.8xlarge instance using a Ubuntu13.04 base AMI. The read count files produced by STAR (unstranded) were used for differential expression analysis using the Bioconductor package edgeR (Robinson et al., 2010). Following calculation of the normalization factors, low-expressing genes were discarded. Counts were then subject to the estimateGLMCommonDisp function followed by glmFit. Differential expression for comparison between phenotypes was then performed using the glmLRT function. ISGs were annotated using the Interferome web tool (http://www.interferome.org/interferome/search/showSearch.jspx), defined as all Type I IFN-regulated genes in all tissues of *Mus musculus* with a cutoff of 3-fold expression. Read count and fastq files are available at SRA. For bioinformatics analysis, we used FunRich software to determine the enrichment of specific biological pathways and transcription factor networks among genes with dysregulated expression in both $Adar^{-/-}$ and $Adar^{-/-}Mavs^{-/-}$ embryos, relative to the representation of these pathways in the genome.

CRISPR targeting of ADAR1 in human cells

For targeting of *ADAR* with CRISPR-Cas9, we used a lentiviral vector in which an RNA polymerase III promoter–driven guide RNA and an RNA polymerase II promoter–driven Cas9-T2A cassette (including sequence encoding a protein for resistance to puromycin) were constitutively expressed from a single, self-inactivating lentivirus upon integration into the host cell genome. Lentivirus pseudotyped with vesicular stomatitis virus envelope glycoprotein was produced by transfection of 2.5×10^6 HEK 293T cells for 48 h in 10-cm plates with 10 μg of the CRISPR-Cas9 *ADAR* targeting construct, 9 μg psPAX-2 (a lentiviral packaging plasmid) and 1 μg pVSV-G (plasmid encoding vesicular stomatitis virus envelope glycoprotein). 2.5×10^6 HEK 293T cells were transduced with the viral supernatants on day 3 after harvest, then were selected for 3 d with 5 μg/ml puromycin (Life Technologies). Subsequent single-cell cloning was performed by serial dilution. Targeting of the *ADAR* locus via CRISPR was evaluated by restriction fragment length polymorphism with an *ApoI* (New England Biolabs) restriction site that overlapped the CRISPR targeting site. Products were separated by electrophoresis through a 3% MetaPhor agarose gel (Lonza). *ADAR* mutations were identified by PCR amplification of the surrounding sequence, cloning into pCDNA3, and sequencing of nine independent plasmids. ADAR1 protein loss was confirmed by immunoblot analysis of whole-cell extracts with or without 24 hours of human IFNβ treatment (100 U/mL, R&D Systems) with rabbit polyclonal anti-ADAR1 (12317; Cell Signaling Technologies) and mouse monoclonal anti-β actin (AC-74; Sigma). The sequences of the guide RNA target sequence is (sense), 5′-GGACAGGAGACGGAATTCGC-3′.

ISRE-luciferase reporter assays

1×10^5 HEK 293T cells with or without ADAR1 expression in 24 well plates were transfected with 25 ng ISRE-luciferase reporter plasmid (Takara Bio Inc.) with 0, 12.5, 25, 50, 100, or 200 ng of pCDNA.3-expressing human RLRs using Lipofectamine® 2000 (Life Technologies) and then incubated for 24 h. Cells were lysed in Passive Lysis Buffer (Promega) and luciferase activity was assessed using the Luciferase Reporter Assay System (Promega) according to the manufacturer's instructions and read using a Centro LB 960 Luminometer (Berthold Technologies).

Statistical Analysis

Statistical significance of difference between groups was assessed using Wilcoxon Rank Sum, Chi Square Goodness-of-fit or two-way ANOVA with Tukey's multiple comparison test, as indicated in the figure legends. Values of $p<0.05$ were considered statistically significant. All analyses were performed using Prism v6.0 software (GraphPad).

Supplementary Material

Refer to Web version on PubMed Central for supplementary material.

Acknowledgments

We are grateful to Stuart Orkin for providing mice with the *Adar* conditional allele; to Ming R. Loo and Michael Gale, Jr for providing *Mavs*$^{-/-}$, *Ifih1*$^{-/-}$, and *Ddx58*$^{-/-}$ mice; to Shizuo Akira for the *Ddx58*$^{-/-}$ mice; to Marco Colonna for the *Ifih1*$^{-/-}$ mice; to Glen Barber for *Tmem173*$^{-/-}$ mice; to M. B. A. Oldstone for *Adar p150*$^{+/-}$ gametes; to Yanick Crow for helpful insights; to Stephanie Cambier for bioinformatics analysis; to Brian Johnson, Kerrie Allen, and the staff of UW Histology and Imaging Core for their technical expertise; and to members of the Stetson and Bevan labs for helpful discussions. DBS is a scholar of the Rita Allen Foundation and a Burroughs Wellcome Fund Investigator in the Pathogenesis of Infectious Disease. This work was supported by grants from the NIH (AI084914-DBS and NDP; T32GM007270-KP), and the Lupus Research Institute (DBS).

References

Ablasser A, Hemmerling I, Schmid-Burgk JL, Behrendt R, Roers A, Hornung V. TREX1 deficiency triggers cell-autonomous immunity in a cGAS-dependent manner. J Immunol. 2014; 192:5993–5997. [PubMed: 24813208]

Aicardi J, Goutieres F. A progressive familial encephalopathy in infancy with calcifications of the basal ganglia and chronic cerebrospinal fluid lymphocytosis. Ann Neurol. 1984; 15:49–54. [PubMed: 6712192]

Bahn JH, Ahn J, Lin X, Zhang Q, Lee JH, Civelek M, Xiao X. Genomic analysis of ADAR1 binding and its involvement in multiple RNA processing pathways. Nature communications. 2015; 6:6355.

Bass BL. RNA editing by adenosine deaminases that act on RNA. Annu Rev Biochem. 2002; 71:817–846. [PubMed: 12045112]

Crow YJ, Chase DS, Lowenstein Schmidt J, Szynkiewicz M, Forte GM, Gornall HL, Oojageer A, Anderson B, Pizzino A, Helman G, et al. Characterization of human disease phenotypes associated with mutations in TREX1, RNASEH2A, RNASEH2B, RNASEH2C, SAMHD1, ADAR, and IFIH1. American journal of medical genetics Part A. 2015; 167A:296–312. [PubMed: 25604658]

Crow YJ, Manel N. Aicardi-Goutieres syndrome and the type I interferonopathies. Nat Rev Immunol. 2015; 15:429–440. [PubMed: 26052098]

Dobin A, Davis CA, Schlesinger F, Drenkow J, Zaleski C, Jha S, Batut P, Chaisson M, Gingeras TR. STAR: ultrafast universal RNA-seq aligner. Bioinformatics. 2013; 29:15–21. [PubMed: 23104886]

Frank MG, Stryker MP, Tecott LH. Sleep and sleep homeostasis in mice lacking the 5-HT2c receptor. Neuropsychopharmacology : official publication of the American College of Neuropsychopharmacology. 2002; 27:869–873. [PubMed: 12431861]

Gall A, Treuting P, Elkon KB, Loo YM, Gale M Jr, Barber GN, Stetson DB. Autoimmunity Initiates in Nonhematopoietic Cells and Progresses via Lymphocytes in an Interferon-Dependent Autoimmune Disease. Immunity. 2012; 36:120–131. [PubMed: 22284419]

Gao D, Li T, Li XD, Chen X, Li QZ, Wight-Carter M, Chen ZJ. Activation of cyclic GMP-AMP synthase by self-DNA causes autoimmune diseases. Proc Natl Acad Sci U S A. 2015

Gateva V, Sandling JK, Hom G, Taylor KE, Chung SA, Sun X, Ortmann W, Kosoy R, Ferreira RC, Nordmark G, et al. A large-scale replication study identifies TNIP1, PRDM1, JAZF1, UHRF1BP1 and IL10 as risk loci for systemic lupus erythematosus. Nat Genet. 2009; 41:1228–1233. [PubMed: 19838195]

Gitlin L, Barchet W, Gilfillan S, Cella M, Beutler B, Flavell RA, Diamond MS, Colonna M. Essential role of mda-5 in type I IFN responses to polyriboinosinic:polyribocytidylic acid and encephalomyocarditis picornavirus. Proc Natl Acad Sci U S A. 2006; 103:8459–8464. [PubMed: 16714379]

Goldstone DC, Ennis-Adeniran V, Hedden JJ, Groom HC, Rice GI, Christodoulou E, Walker PA, Kelly G, Haire LF, Yap MW, et al. HIV-1 restriction factor SAMHD1 is a deoxynucleoside triphosphate triphosphohydrolase. Nature. 2011; 480:379–382. [PubMed: 22056990]

Goubau D, Deddouche S, Reis ESC. Cytosolic sensing of viruses. Immunity. 2013; 38:855–869. [PubMed: 23706667]

Gray EE, Treuting PM, Woodward JJ, Stetson DB. Cutting Edge: cGAS Is Required for Lethal Autoimmune Disease in the Trex1-Deficient Mouse Model of Aicardi-Goutieres Syndrome. J Immunol. 2015; 195:1939–1943. [PubMed: 26223655]

Hartner JC, Schmittwolf C, Kispert A, Muller AM, Higuchi M, Seeburg PH. Liver disintegration in the mouse embryo caused by deficiency in the RNA-editing enzyme ADAR1. J Biol Chem. 2004; 279:4894–4902. [PubMed: 14615479]

Hartner JC, Walkley CR, Lu J, Orkin SH. ADAR1 is essential for the maintenance of hematopoiesis and suppression of interferon signaling. Nat Immunol. 2009; 10:109–115. [PubMed: 19060901]

Hayashi M, Suzuki T. Dyschromatosis symmetrica hereditaria. The Journal of dermatology. 2013; 40:336–343. [PubMed: 22974014]

Hiller B, Achleitner M, Glage S, Naumann R, Behrendt R, Roers A. Mammalian RNase H2 removes ribonucleotides from DNA to maintain genome integrity. J Exp Med. 2012; 209:1419–1426. [PubMed: 22802351]

Hrecka K, Hao C, Gierszewska M, Swanson SK, Kesik-Brodacka M, Srivastava S, Florens L, Washburn MP, Skowronski J. Vpx relieves inhibition of HIV-1 infection of macrophages mediated by the SAMHD1 protein. Nature. 2011; 474:658–661. [PubMed: 21720370]

Ishikawa H, Ma Z, Barber GN. STING regulates intracellular DNA-mediated, type I interferon-dependent innate immunity. Nature. 2009; 461:788–792. [PubMed: 19776740]

Kato H, Sato S, Yoneyama M, Yamamoto M, Uematsu S, Matsui K, Tsujimura T, Takeda K, Fujita T, Takeuchi O, Akira S. Cell type-specific involvement of RIG-I in antiviral response. Immunity. 2005; 23:19–28. [PubMed: 16039576]

Kato H, Takeuchi O, Sato S, Yoneyama M, Yamamoto M, Matsui K, Uematsu S, Jung A, Kawai T, Ishii KJ, et al. Differential roles of MDA5 and RIG-I helicases in the recognition of RNA viruses. Nature. 2006; 441:101–105. [PubMed: 16625202]

Laguette N, Sobhian B, Casartelli N, Ringeard M, Chable-Bessia C, Segeral E, Yatim A, Emiliani S, Schwartz O, Benkirane M. SAMHD1 is the dendritic- and myeloid-cell-specific HIV-1 restriction factor counteracted by Vpx. Nature. 2011; 474:654–657. [PubMed: 21613998]

Lebon P, Badoual J, Ponsot G, Goutieres F, Hemeury-Cukier F, Aicardi J. Intrathecal synthesis of interferon-alpha in infants with progressive familial encephalopathy. J Neurol Sci. 1988; 84:201–208. [PubMed: 2837539]

Liddicoat BJ, Piskol R, Chalk AM, Ramaswami G, Higuchi M, Hartner JC, Li JB, Seeburg PH, Walkley CR. RNA editing by ADAR1 prevents MDA5 sensing of endogenous dsRNA as nonself. Science. 2015; 349:1115–1120. [PubMed: 26275108]

Livingston JH, Lin JP, Dale RC, Gill D, Brogan P, Munnich A, Kurian MA, Gonzalez-Martinez V, De Goede CG, Falconer A, et al. A type I interferon signature identifies bilateral striatal necrosis due to mutations in ADAR1. J Med Genet. 2014; 51:76–82. [PubMed: 24262145]

Mannion NM, Greenwood SM, Young R, Cox S, Brindle J, Read D, Nellaker C, Vesely C, Ponting CP, McLaughlin PJ, et al. The RNA-editing enzyme ADAR1 controls innate immune responses to RNA. Cell reports. 2014; 9:1482–1494. [PubMed: 25456137]

Nejentsev S, Walker N, Riches D, Egholm M, Todd JA. Rare Variants of IFIH1, a Gene Implicated in Antiviral Responses, Protect Against Type 1 Diabetes. Science. 2009; 324:387–389. [PubMed: 19264985]

Osenberg S, Paz Yaacov N, Safran M, Moshkovitz S, Shtrichman R, Sherf O, Jacob-Hirsch J, Keshet G, Amariglio N, Itskovitz-Eldor J, Rechavi G. Alu sequences in undifferentiated human

embryonic stem cells display high levels of A-to-I RNA editing. PLoS One. 2010; 5:e11173. [PubMed: 20574523]

Ota H, Sakurai M, Gupta R, Valente L, Wulff BE, Ariyoshi K, Iizasa H, Davuluri RV, Nishikura K. ADAR1 forms a complex with Dicer to promote microRNA processing and RNA-induced gene silencing. Cell. 2013; 153:575–589. [PubMed: 23622242]

Rehwinkel J, Maelfait J, Bridgeman A, Rigby R, Hayward B, Liberatore RA, Bieniasz PD, Towers GJ, Moita LF, Crow YJ, et al. SAMHD1-dependent retroviral control and escape in mice. Embo J. 2013; 32:2454–2462. [PubMed: 23872947]

Reijns MA, Rabe B, Rigby RE, Mill P, Astell KR, Lettice LA, Boyle S, Leitch A, Keighren M, Kilanowski F, et al. Enzymatic removal of ribonucleotides from DNA is essential for mammalian genome integrity and development. Cell. 2012; 149:1008–1022. [PubMed: 22579044]

Rice GI, del Toro Duany Y, Jenkinson EM, Forte GM, Anderson BH, Ariaudo G, Bader-Meunier B, Baildam EM, Battini R, Beresford MW, et al. Gain-of-function mutations in IFIH1 cause a spectrum of human disease phenotypes associated with upregulated type I interferon signaling. Nat Genet. 2014; 46:503–509. [PubMed: 24686847]

Rice GI, Kasher PR, Forte GM, Mannion NM, Greenwood SM, Szynkiewicz M, Dickerson JE, Bhaskar SS, Zampini M, Briggs TA, et al. Mutations in ADAR1 cause Aicardi-Goutieres syndrome associated with a type I interferon signature. Nat Genet. 2012; 44:1243–1248. [PubMed: 23001123]

Robinson MD, McCarthy DJ, Smyth GK. edgeR: a Bioconductor package for differential expression analysis of digital gene expression data. Bioinformatics. 2010; 26:139–140. [PubMed: 19910308]

Ruzankina Y, Pinzon-Guzman C, Asare A, Ong T, Pontano L, Cotsarelis G, Zediak VP, Velez M, Bhandoola A, Brown EJ. Deletion of the developmentally essential gene ATR in adult mice leads to age-related phenotypes and stem cell loss. Cell stem cell. 2007; 1:113–126. [PubMed: 18371340]

Schwartz T, Rould MA, Lowenhaupt K, Herbert A, Rich A. Crystal structure of the Zalpha domain of the human editing enzyme ADAR1 bound to left-handed Z-DNA. Science. 1999; 284:1841–1845. [PubMed: 10364558]

Smyth DJ, Cooper JD, Bailey R, Field S, Burren O, Smink LJ, Guja C, Ionescu-Tirgoviste C, Widmer B, Dunger DB, et al. A genome-wide association study of nonsynonymous SNPs identifies a type 1 diabetes locus in the interferon-induced helicase (IFIH1) region. Nat Genet. 2006; 38:617–619. [PubMed: 16699517]

Spandidos A, Wang X, Wang H, Seed B. PrimerBank: a resource of human and mouse PCR primer pairs for gene expression detection and quantification. Nucleic Acids Res. 2010; 38:D792–799. [PubMed: 19906719]

Stetson DB, Ko JS, Heidmann T, Medzhitov R. Trex1 prevents cell-intrinsic initiation of autoimmunity. Cell. 2008; 134:587–598. [PubMed: 18724932]

Sutherland A, Davies J, Owen CJ, Vaikkakara S, Walker C, Cheetham TD, James RA, Perros P, Donaldson PT, Cordell HJ, et al. Genomic polymorphism at the interferon-induced helicase (IFIH1) locus contributes to Graves' disease susceptibility. The Journal of clinical endocrinology and metabolism. 2007; 92:3338–3341. [PubMed: 17535987]

Tecott LH, Sun LM, Akana SF, Strack AM, Lowenstein DH, Dallman MF, Julius D. Eating disorder and epilepsy in mice lacking 5-HT2c serotonin receptors. Nature. 1995; 374:542–546. [PubMed: 7700379]

Vitali P, Scadden AD. Double-stranded RNAs containing multiple IU pairs are sufficient to suppress interferon induction and apoptosis. Nat Struct Mol Biol. 2010; 17:1043–1050. [PubMed: 20694008]

Wang IX, So E, Devlin JL, Zhao Y, Wu M, Cheung VG. ADAR regulates RNA editing, transcript stability, and gene expression. Cell reports. 2013; 5:849–860. [PubMed: 24183664]

Wang Q, Khillan J, Gadue P, Nishikura K. Requirement of the RNA editing deaminase ADAR1 gene for embryonic erythropoiesis. Science. 2000; 290:1765–1768. [PubMed: 11099415]

Ward SV, George CX, Welch MJ, Liou LY, Hahm B, Lewicki H, de la Torre JC, Samuel CE, Oldstone MB. RNA editing enzyme adenosine deaminase is a restriction factor for controlling

measles virus replication that also is required for embryogenesis. Proc Natl Acad Sci U S A. 2011; 108:331–336. [PubMed: 21173229]

Wu B, Peisley A, Richards C, Yao H, Zeng X, Lin C, Chu F, Walz T, Hur S. Structural basis for dsRNA recognition, filament formation, and antiviral signal activation by MDA5. Cell. 2013; 152:276–289. [PubMed: 23273991]

Wu J, Chen ZJ. Innate immune sensing and signaling of cytosolic nucleic acids. Annu Rev Immunol. 2014; 32:461–488. [PubMed: 24655297]

Yang S, Deng P, Zhu Z, Zhu J, Wang G, Zhang L, Chen AF, Wang T, Sarkar SN, Billiar TR, Wang Q. Adenosine deaminase acting on RNA 1 limits RIG-I RNA detection and suppresses IFN production responding to viral and endogenous RNAs. J Immunol. 2014; 193:3436–3445. [PubMed: 25172485]

Yang W, Chendrimada TP, Wang Q, Higuchi M, Seeburg PH, Shiekhattar R, Nishikura K. Modulation of microRNA processing and expression through RNA editing by ADAR deaminases. Nat Struct Mol Biol. 2006; 13:13–21. [PubMed: 16369484]

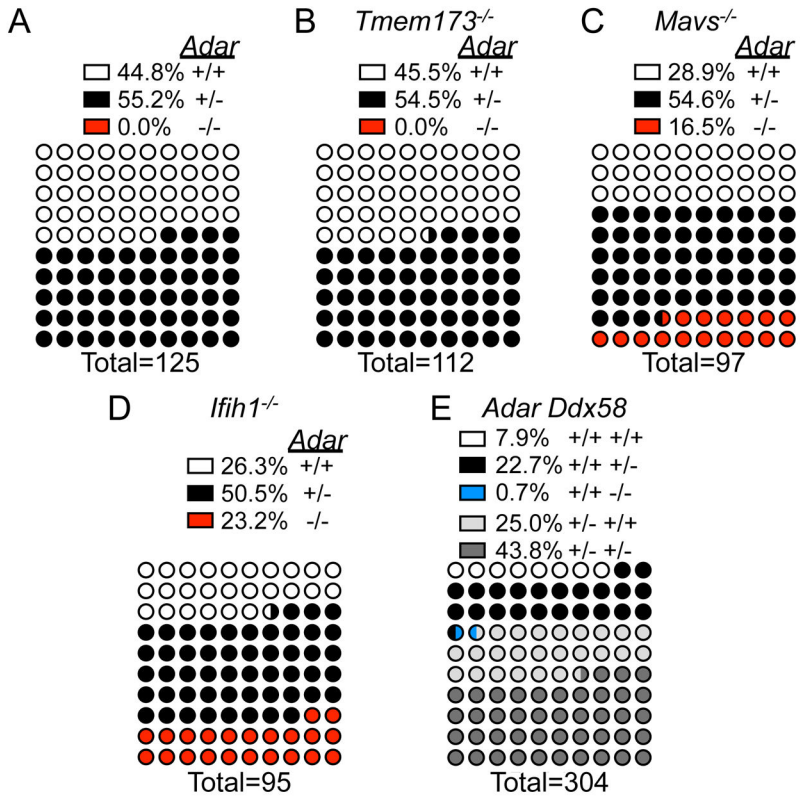

Figure 1. Rescue of *Adar*−/− mice to birth by Ifih1/Mda5 and MAVS deficiency

(A) Live births from $Adar^{+/-}$ intercross.

(B) Live births from $Adar^{+/-}Tmem173^{-/-}$ intercross.

(C) Live births from $Adar^{+/-}Mavs^{-/-}$ intercross.

(D) Live births from $Adar^{+/-}Ifih1^{-/-}$ intercross.

(E) Live births from $Adar^{+/-}Ddx58^{+/-}$ intercross. Percent rescue $p>0.05$ by Chi Square goodness-of-fit for $Adar^{+/-}Mavs^{-/-}$ intercross and $Adar^{+/-}Ifih1^{-/-}$ intercross.

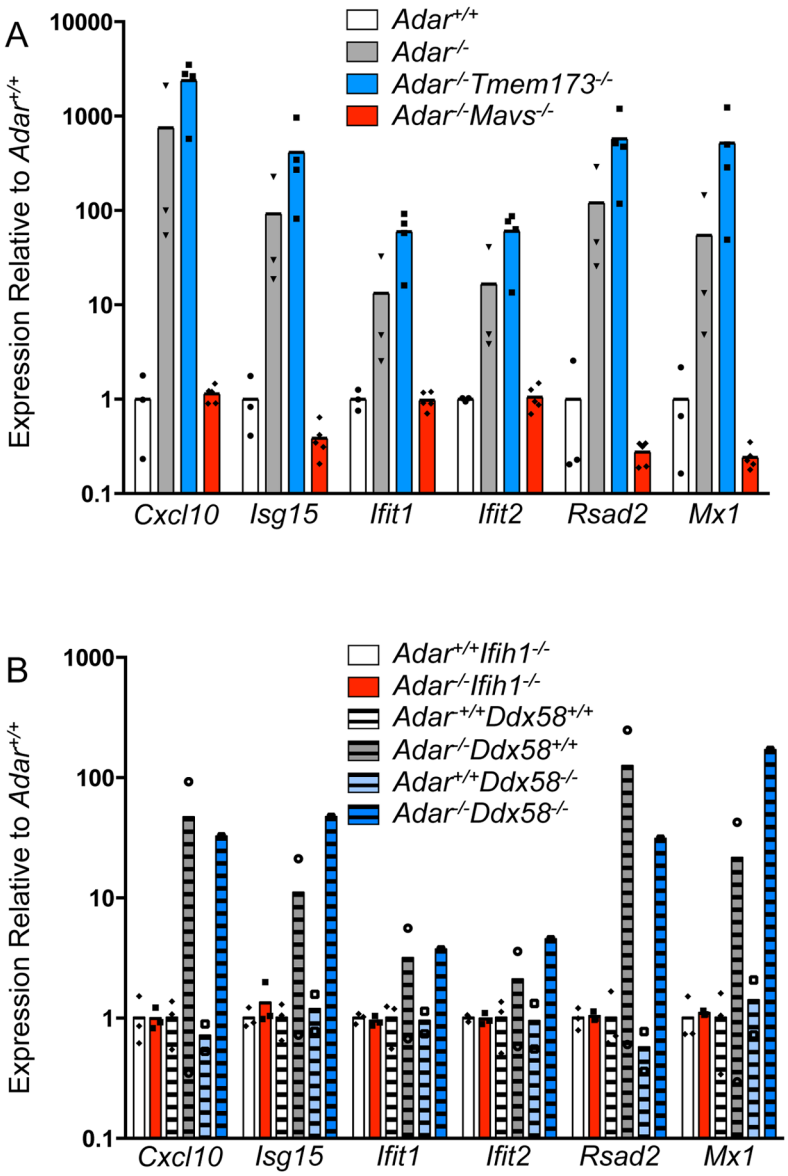

Figure 2. MDA5 and MAVS deficiency reverse the IFN signature in *Adar*−/− embryos

Quantitative RT-PCR on a panel of 6 ISGs from whole E11.5 embryos.

(A) *Adar*$^{+/+}$ (white, n=3), *Adar*$^{-/-}$ (grey, n=3), *Adar*$^{-/-}$*Sting*$^{-/-}$ (blue, n=4), *Adar*$^{-/-}$*Mavs*$^{-/-}$ (red, n=5). Interferon signature assessed by Wilcoxon Signed Rank test compared to *Adar*$^{+/+}$: Adar$^{-/-}$ p=0.03, *Adar*$^{-/-}$*Sting*$^{-/-}$ p=0.03, *Adar*$^{-/-}$*Mavs*$^{-/-}$ p=0.31.

(B) *Adar*$^{+/+}$*Ifih1*$^{-/-}$ (white, n=3), *Adar*$^{-/-}$*Ifih1*$^{-/-}$ (red, n=3), *Adar*$^{-+/+}$*Ddx58*$^{+/+}$ (white stripes, n=3), *Adar*$^{--/-}$*Ddx58*$^{+/+}$ (grey stripes, n=2), *Adar*$^{+/+}$*Ddx58*$^{-/-}$ (light blue stripes, n=2), *Adar*$^{--/-}$*Ddx58*$^{-/-}$ (blue stripes, n=1). Interferon signature assessed by Wilcoxon Signed Rank test compare to *Adar*$^{+/+}$controls, *Adar*$^{-/-}$*Ifih1*$^{-/-}$ p=0.56, *Adar*$^{--/-}$*Ddx58*$^{+/+}$ p=0.03, *Adar*$^{+/+}$*Ddx58*$^{-/-}$ p=0.69, *Adar*$^{--/-}$*Ddx58*$^{-/-}$ p=0.03.

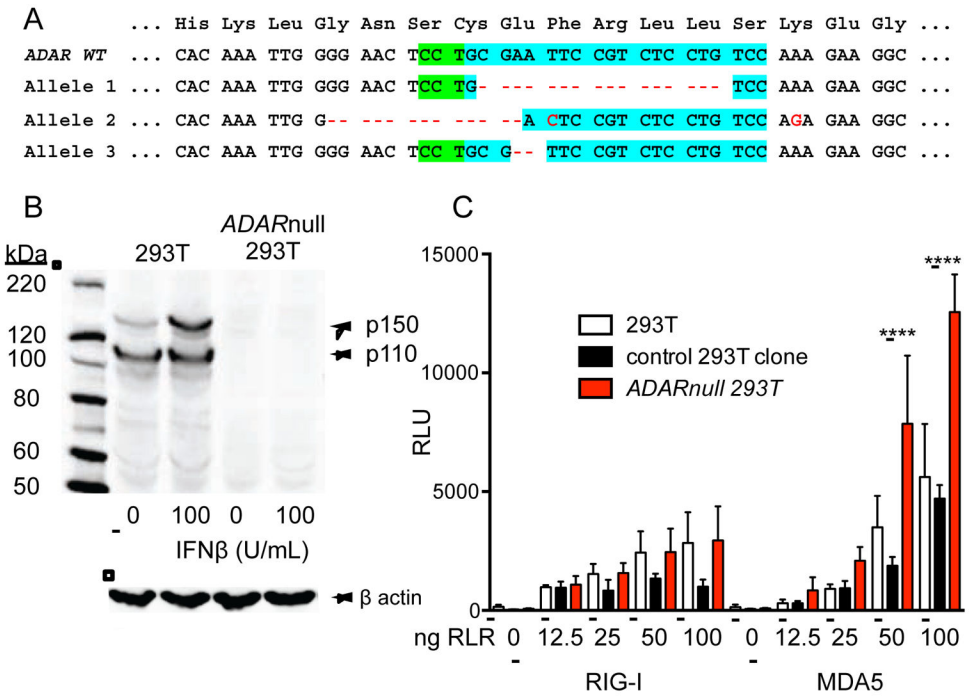

Figure 3. ADAR1 specifically regulates the MDA5 pathway in human cells

(A) Generation of *ADAR*-null HEK 293T cells by lentiCRISPR targeting. The CRISPR target site in exon 4 of the *ADAR* gene is indicated in blue, and the protospacer adjacent motif (PAM) is shown in green. The Cas9 cleavage site is indicated with an arrow. Deletions in the three *ADAR* alleles, each of which results in a frameshift, are shown by the red dashes.

(B) Western blot of ADAR1 protein using lysates from control HEK 293T cells and an *ADAR*-lentiCRISPR-targeted clone of HEK 293T cells.

(C) The indicated HEK 293T cells were transfected with 25ng ISRE-luciferase reporter plasmid, with or without the indicated amounts of plasmids encoding RIG-I or MDA5. Cells were analyzed for relative luciferase units 24 hours after transfection. Mean±SD; ***: $p<0.0001$ in Two way ANOVA test with Tukey's multiple comparison. Data are representative of 4 independent experiments.

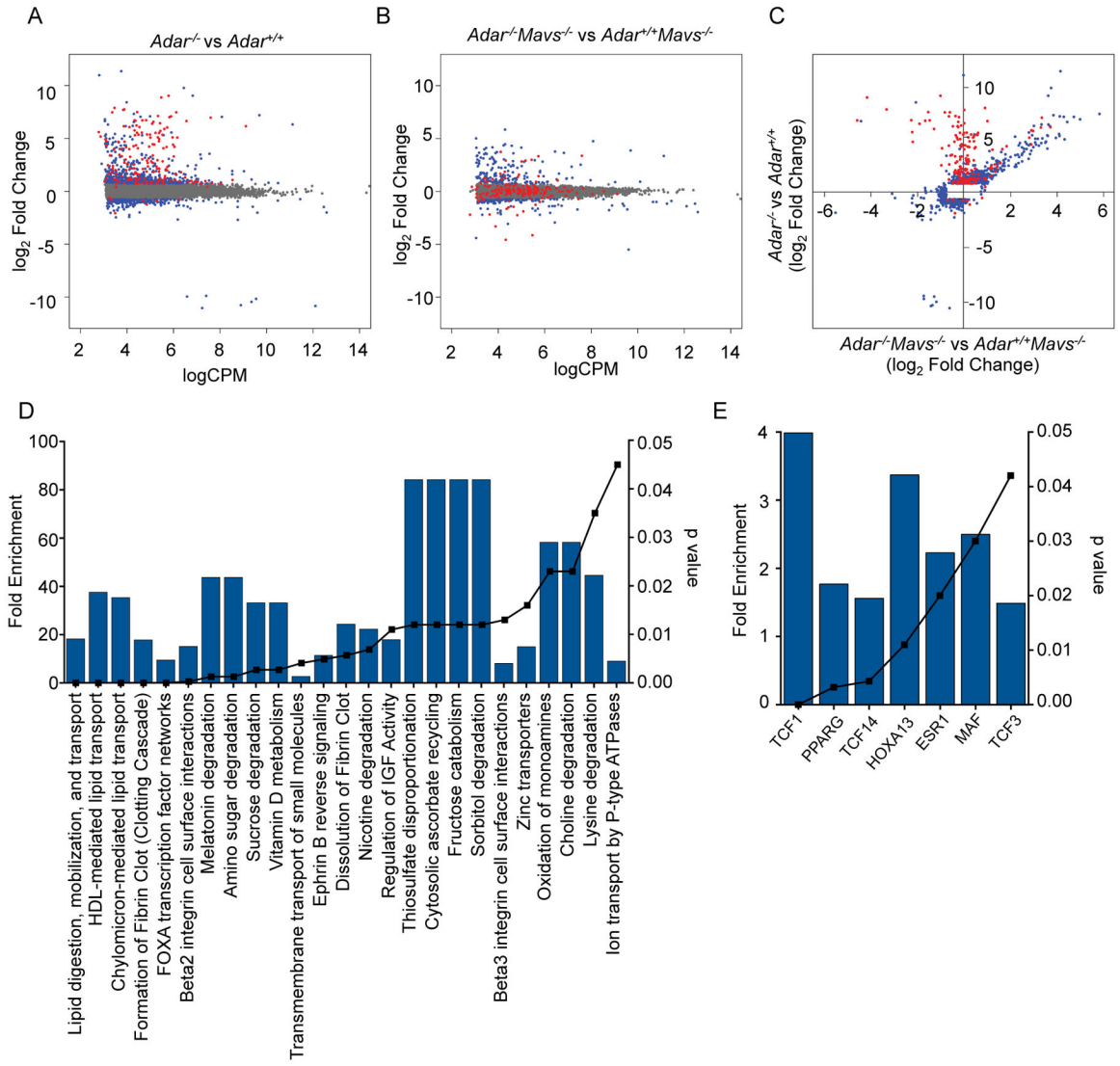

Figure 4. MAVS-dependent and MAVS-independent gene expression in *Adar*−/− embryos

RNA-Seq was performed on rRNA-depleted RNA from whole E11.5 embryos of the indicated genotypes.

(A) Comparison of gene expression between *Adar*$^{-/-}$ (n=3) and *Adar*$^{+/+}$ (n=3) embryos. Data are plotted as $\log_2$ fold change in gene expression on the y-axis, with normalized $\log_2$ counts per million (CPM) on the x-axis. Grey dots denote genes with insignificant differences in expression. Blue dots denote non-ISGs with differential expression ($p \leq 0.01$). Red dots indicate ISGs with differential expression ($p \leq 0.01$).

(B) Comparison of gene expression between *Adar*$^{-/-}$*Mavs*$^{-/-}$ (n=3) and *Mavs*$^{-/-}$ (n=3) embryos, using the same criteria as in (A).

(C) Genes with differential expression ($p \leq 0.01$) in either pairwise comparison were plotted, with *Adar*$^{-/-}$ vs. *Adar*$^{+/+}$ on the y-axis, and *Adar*$^{-/-}$*Mavs*$^{-/-}$ vs. *Mavs*$^{-/-}$ on the x-axis. Blue and red genes are the same as (A) and (B).

(D) Biological pathways enriched among the genes with dysregulated expression in both *Adar*$^{-/-}$ embryos and *Adar*$^{-/-}$*Mavs*$^{-/-}$embryos identified in (C).

(E) Transcription factor binding sites enriched among the MAVS-independent differentially expressed genes from (C).

For D and E, fold enrichment relative to the representation of these pathways in the genome is shown on the left y-axis and the blue bars. Significance of enrichment is indicated by hyper geometric p-value on the right y-axis and the black symnbols/line. Analysis was performed using FunRich software.

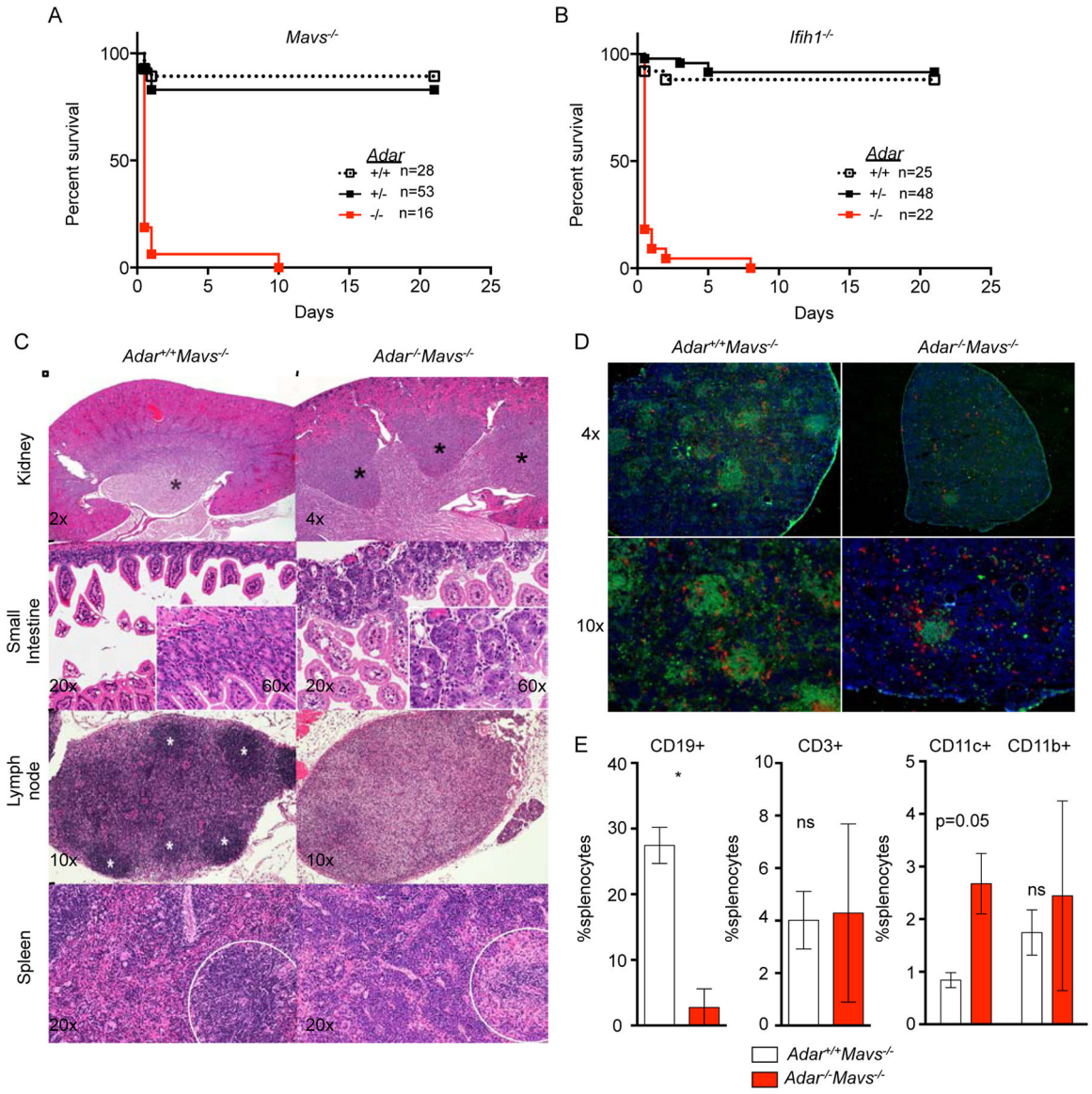

Figure 5. Postnatal mortality and severe developmental defects in *Adar−/−Mavs−/−* mice

(A) Postnatal survival curves for $Adar^{-/-}Mavs^{-/-}$ mice.

(B) Postnatal survival curves for $Adar^{-/-}Ifih1^{-/-}$ mice.

(C) $Adar^{-/-}$; $Mavs^{-/-}$ mice have developmental defects of the kidney (top row; papillae marked with black asterisks), small intestine (second row), lymph node (third row; follicles marked with white asterisks), and spleen (fourth row; lymphoid regions enclosed by dashed circle). Images are hematoxylin and eosin with magnification indicated.

(D) Immunofluorescence microscopy of splenic sections with anti-B220 (green), anti-CD8 and anti-CD4 (red), and DAPI (blue).

(E) Analysis of splenocytes by flow cytometry shows severe B cell deficiency in $Adar^{-/-}$; $Mavs^{-/-}$ mice. Mice in C-D were 20 days old. Mice in E were 15 days old. Mice in F were 13 days old.

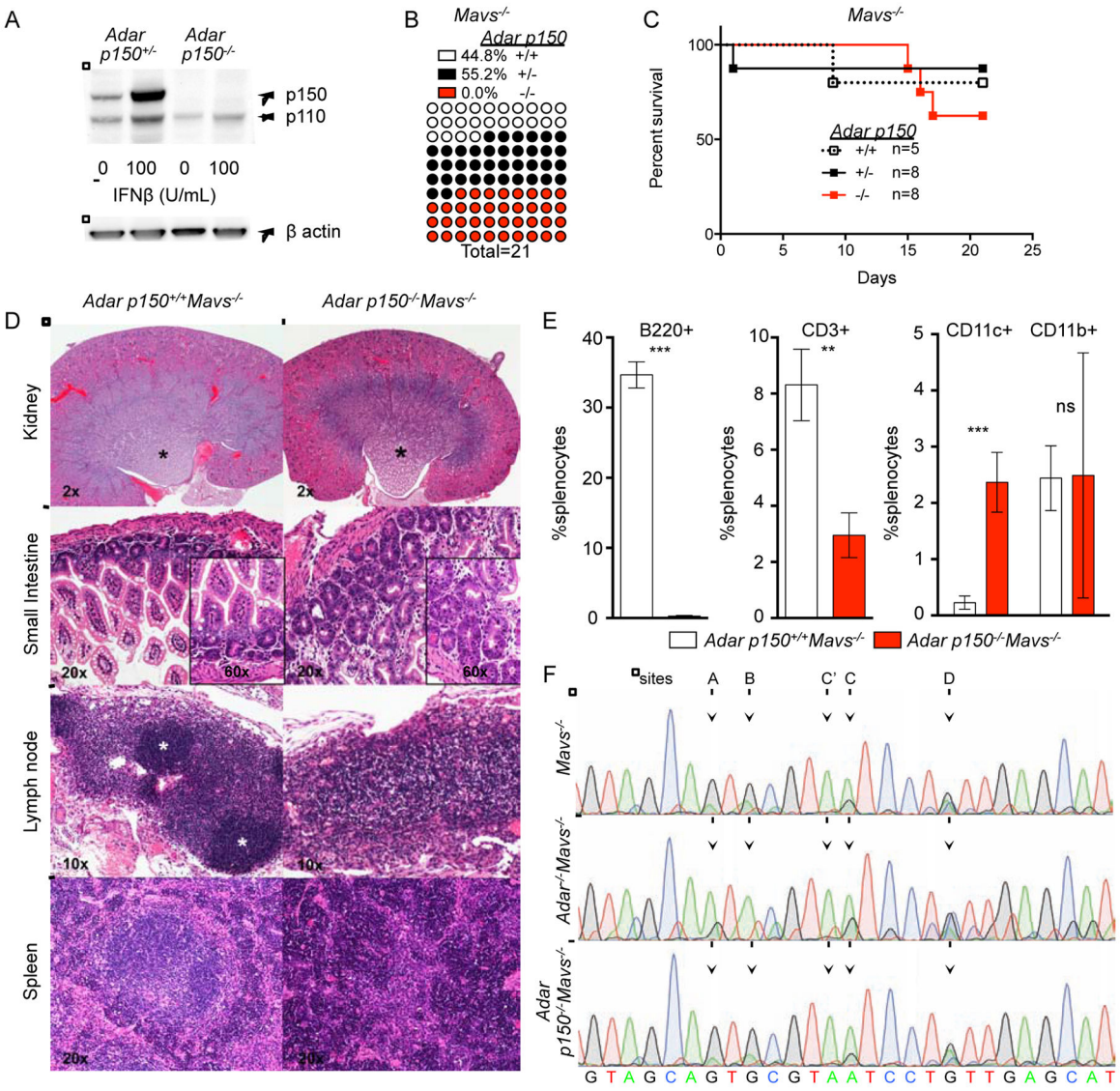

Figure 6. Independent roles for ADAR1 isoforms in regulation of MDA5-MAVS and development

(A) Western blot of ADAR1 protein expression in $p150^{+/-}$ or $p150^{-/-}$ MEFs.

(B) Live births for mice from the $p150^{+/-}Mavs^{-/-}$ intercross.

(C) Postnatal survival curves for mice from the $p150^{+/-}Mavs^{-/-}$ intercross.

(D) Hematoxylin and eosin-stained tissue sections of the indicated organs of $p150^{-/-}$; $Mavs^{-/-}$ mice and controls are shown, with magnification indicated.

(E) Analysis of splenocytes by flow cytometry shows severe B cell deficiency and an increase in CD11c+ myeloid cells in $p150^{-/-}Mavs^{-/-}$ mice. Two sample t-test for p values $p150^{+/+}Mavs^{-/-}$ n=3, $p150^{-/-}Mavs^{-/-}$ n=3 *** p<0.002, **p=0.004.

(F) Representative chromatograms of 2-HT2C receptor transcript editing in brains of 15–21 day old mice of the indicated genotypes. Mice in E and F were 21 days old. Mice in D were 15 days old.

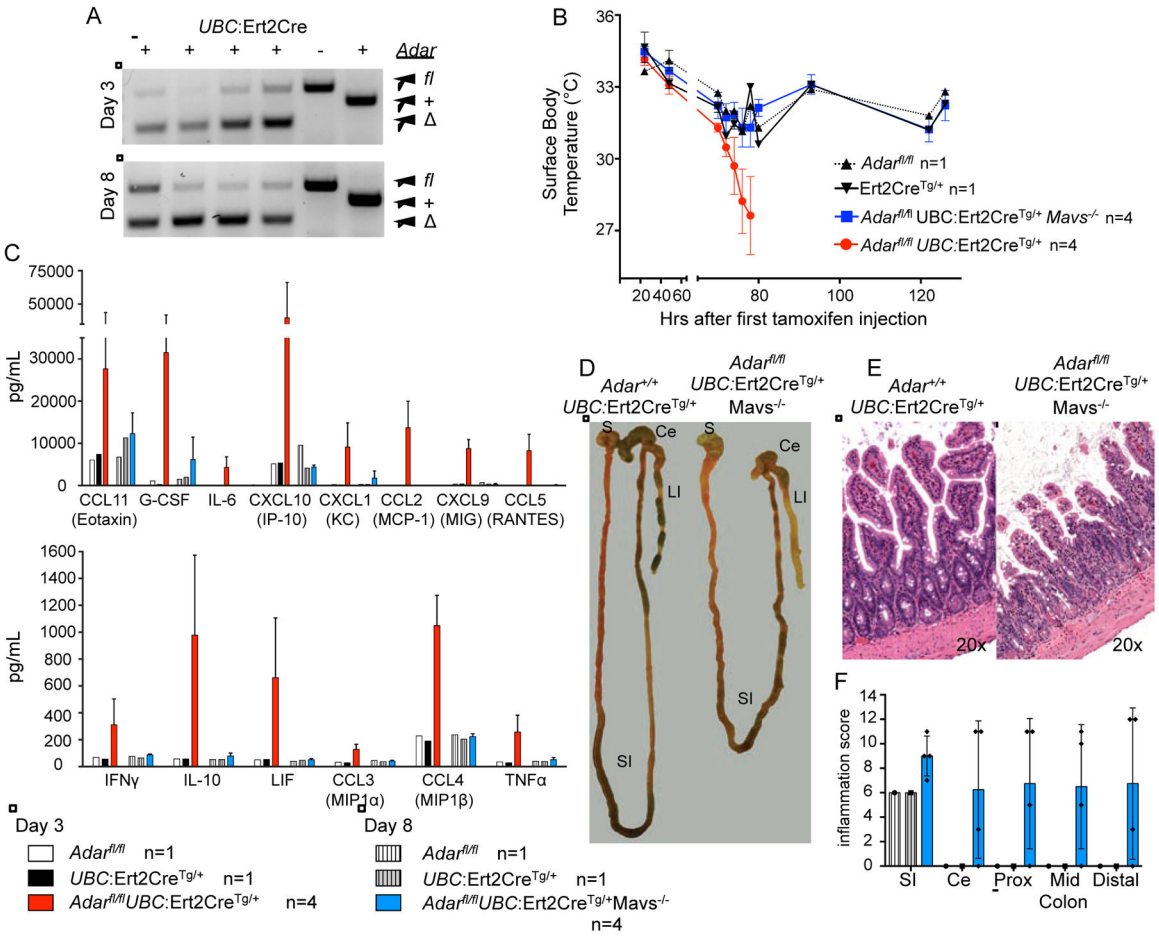

Figure 7. ADAR1 regulates both the MDA5-MAVS pathway and tissue homeostasis in adults

Mice were treated with 2 mg tamoxifen i.p. daily for 3 days and observed for gross pathology.

(A) Samples of the ear were genotyped for *Adar* deletion following tamoxifen treatment.

(B) Surface body temperate readings for tamoxifen-treated mice from 20–120 hours after initial tamoxifen injection.

(C) Serum cytokine levels determined from mice at Day 3 or Day 8.

(D) *Ex vivo* dissection of the gastrointestinal tract at Day 8; Stomach (S), small intestine (SI), cecum (Ce) and large intestine (LI) are indicated.

(E) Representative hematoxylin and eosin-stained ileum sections of tamoxifen-treated mice of the indicated genotypes at Day 8. Original magnification is indicated in the bottom right.

(F) Histological scoring of inflammation in the gut at Day 8. SI=small intestine; CE=cecum; Prox=Proximal colon; Mid=Mid-colon. Mean inflammation score of $Adar^{fl/fl}Mavs^{-/-}$ *UBC:Ert2Cre+* intestines compared to either control is significant by one-way ANOVA, p=0.002.